fibers

MDPI

Article

DAMAGE CHARACTERIZATION OF NANOINTERLEAVED CFRP UNDER STATIC AND FATIGUE LOADING

Mohamad Fotouhi[1]*, Cristiano Fragassa[2], Sakineh Fotouhi[3], Hamed Saghafi[4], Giangiacomo Minak[4]

[1] Department of Design and Mathematics; The University of the West of England; Bristol BS16 1QY; UK;
[2] Department of Industrial Engineering, University of Bologna, Viale Risorgimento 2, 40136 Bologna, Italy
[3] Mechanical Engineering Department; University of Tabriz; Tabriz; Iran
[4] Department of Mechanical Engineering; Tafresh University, Tehran Road; 7961139518; Tafresh; Iran
* Correspondence: mohammad.fotouhi@uwe.ac.uk; Tel.: +447407266470

Received: date; Accepted: date; Published: date

Abstract: The use of high strength to weight ratio laminated fiber-reinforced composites is emerging in engineering sectors such as aerospace, marine and automotive to improve productivity. Nevertheless, delamination between the layers is a limiting factor for the wider application of laminated composites, as it reduces the stiffness and strengths of the structure. Previous studies have proven that ply interface nanofibrous fiber reinforcement has an effective influence on delamination resistance of laminated composites materials. This paper aims to investigate the effect of nanofiber ply interface reinforcement on mode I properties and failure responses when subjected to static and fatigue loadings. For this purpose, virgin and nanomodified woven laminates were subjected to Double Cantilever Beam (DCB) specimens. Static and fatigue tests were performed and the acoustic emission data were acquired during the tests. The results showed a 130% increase of delamination toughness for nanomodified specimens in the static loadings and more crack growth resistance in the fatigue loading. The AE results showed that different types of failure mechanisms were the cause of these improvements for the nanomodified composites compared with the virgin ones.

Keywords: Nanofibers; Composites; Interleaving; Fatigue; Delamination; Acoustic Emission; Failure Mechanisms.

1. Introduction

Carbon fiber reinforced polymer (CFRP) composites have many applications in different sectors, such as aerospace, superstructure of ships, automotive, civil engineering and sports goods, due to their high strength-to-weight ratio and rigidity. CFRP are usually produced by stacking several sheets of prepregs together. Unlike the excellent in-plane properties of CFRP, they suffer from damage between the plies such as delamination or cracks, which happen mostly in the matrix areas [1–5].

Different methods such as matrix toughening, stitching of the plies, and three-dimensional woven fabrics have been used to prevent delamination. Matrix-toughening has recently attracted a lot of attention at which delamination toughness increases by using toughened material layers during the manufacturing [6-8]. A lot of works have been done on toughening laminated composites using nanofibers interleaving and the overall conclusion was that nanofibers can bring significant benefits to the composite under certain conditions of resin-polymer compatibility, size and amount of

interleave, and type of material [9–11]. New observations showed that mode I fracture toughness of epoxy-resin composites increased with the use of Nylon 66 nanofibers [12, 13] both in static and fatigue loading conditions, if they are treated in a defined condition such as appropriate selection of thickness of nanofibrous and curing temperature.

The aim of this paper is to identify failure mechanisms in the Nylon 66 nanofibers-interleaved composites under static and fatigue loadings. Acoustic Emission (AE) technique was used to monitor the generated AE signals originated from the failure mechanisms during static and fatigue loadings of the Nylon 66 nanofiber-interleaved laminates. AE technique was used to identify the damage types in laminated composite and it has been a useful and applicable method [14-21]. AE signal is an intrinsic energy that is generated during various damage mechanisms under loading condition.

This paper reports a good correlation between the mechanical data and recorded AE signals that were obtained from the experiments on CFRP interleaved with the Nylon 66 nanofibers under both static and fatigue mode I interlaminar loadings.

2. Materials and Methods

Two types of samples, i.e. virgin and nano-interleaved, were fabricated and tested. The samples were made from 14 plies of plain weave (PW) carbon-epoxy prepreg (GG204P-IMP503Z), with 220 gcm, which were stacked together. The prepreg was supplied by Impregnatex Composite Srl (Milan, Italy). The virgin and nano-interleaved laminates were cut from two rectangular panels (300*170 mm^2) that were cured in an autoclave at 60°C cycle for 2 hours and 130°C cycle for 1 hour, with 6 bar pressure, below Nylon's melting temperature which is 260°C. Later the rectangular plates were cut to the size of the test samples according to ASTM D5528 standard [23] as illustrated in Figure 1. The only difference between the virgin and nano-interleaved samples was the addition of a Nylon 66 nanofiber mat between plies 7 and 8 in the nano-interleaved samples. This nanofibre mat had a 40 μm thickness, 18 g/m^2 areal density and 400 to 650 nm diameter nanofibers. Electrospinning technology (see Figure 1a for the schematic) was used to fabricate the Nylon 66 nanofiber mats. Electrospun non-woven mats were fabricated using an in-house electrospinning apparatus (Figure 1A) composed of: (1) a high voltage power supply, (2) a syringe pump (KDScientific 200 series), (3) four syringes, (4) four Teflon tubes, (5) four needles with diameter of 0.6 mm and (6) a grounded rotating collector (length = 500 mm, diameter = 160 mm) which position relative to needles can be changed. The electrospinning process was carried out at room temperature and under applied voltage of 12 kV, feed rate of 0.01 mL/min and 120 mm was the distance between the collector and tip of the needle. More details regarding the manufacturing process of the composite samples can be found in our previously published paper [13].

Although the nano-fibre mat had a 40 μm thickness, but no thickness difference was observed between the nano-interleaved and virgin samples after the curing process and their thickness was measured as 3.5±0.1 mm.

As illustrated in Figures 1c and 1d, ASTM D5528 standard was followed in fabrication and testing of the virgin and nano-interleaved DCB specimens [23].

The quasi-static experiments were done in an Instron 8033 (a servo presses machine) with a 250 N load level, using displacement controlled system with a fixed crosshead speed of 3 mm/min. The load and displacement data was captured by the Instron machine and the crack length was measured by an optical microscope. Modified Beam Theory (MBT) recommended in [23] was used to evaluate energy release rate in mode I.

The fatigue samples were identical to the static samples. A naturally developed fatigued crack with 1mm length was created within the specimens prior to the main fatigue tests. This was done by applying cyclic load and producing a 1 mm crack length before the main fatigue tests. ASTM D6115 was used for the Fatigue tests [24] and the experiments were done by the same machine used for the static tests, with a 200 N load cell, under 3 Hz load frequency and in displacement control mode, with max/min ratio of R=0.3 . Load, displacement and crack length values were used to evaluate Gmax as

suggested in [25]. Three samples were tested for the quasi-static test and just one sample was tested for each fatigue condition.

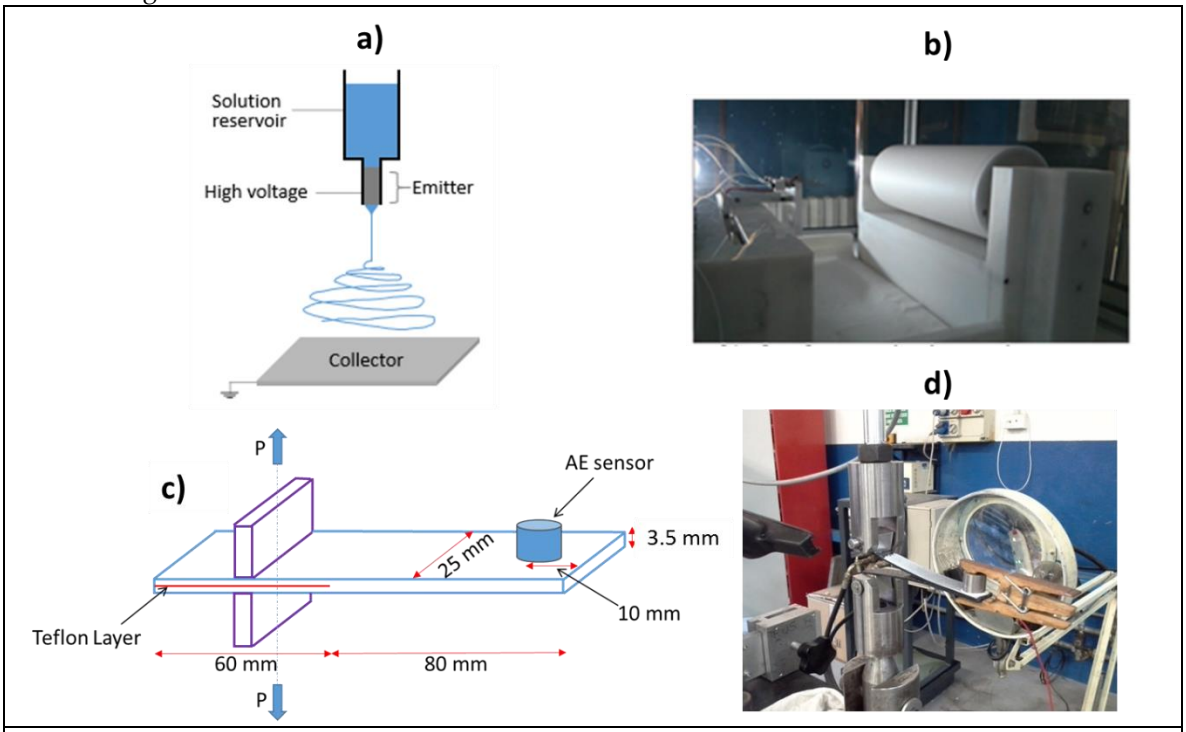

Figure 1. Electrospinning and testing equipment: (a) Schematic of the electrospinning process. (b) The electrospinning equipment. (c) Schematic of the DCB specimens. (d) DCB specimens and experimental setup.

PCI-2 AE system was used to record the AE wave forms with a sampling rate of 10 MHz. Figure 2 shows a schematic of AE wave form and its parameters. A piezoelectric sensor (PAC R15) was used to record the AE signals. A preamplifier (2/4/6-AST) with the gain selector of the 40 dB and 35 dB threshold was used. Calibration of the sensors was done with a pencil lead break test. The AE signal parameters that contain amplitude, duration, counts, rise time, energy, etc. was calculated by AE software (AEWin).

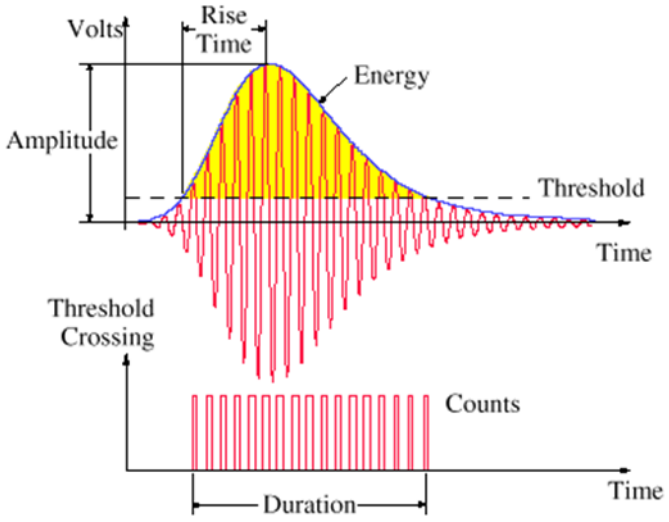

Figure 2. The definitions for acoustic-emission parameters [26].

3. Results and discussion

3.1. Mechanical results

Load-displacement curves for the nano-interleaved and virgin samples are illustrated in Figure 3. The energy release rates are calculated using Equation (1) and are reported in Figure 4. In Equation (1), G_{Ic} is the critical energy release rate, P is the applied load, B is specimen's width, a is the pre-crack length and Δ is the crack growth. For the fatigue samples, the energy release rates are calculated at the peak value of different number of cycles using Equation (1). The results are clearly showing improvement in the fracture toughness for both static and fatigue loadings.

$$G_{Ic} = \frac{3P\delta}{2B(a+\Delta)} \qquad \text{Equation (1)}$$

As summarized in table 1, the nano-interleaved samples have shown a 137% and a 124% increase of G_{IC}, compared to the virgin samples. The fracture toughness is improved at both crack initiation and propagation for the fatigue tests as illustrated in Figure 4.

Table 1. Fracture parameters obtained from mode I fracture tests.

GIC (J/m2) measured based on ASTM D5528			
Methods	Non-linearity method	Visual inspection method	5%/max
Virgin	340±15	385±20	415±25
Nano-interleaved	790±30	860±50	1000±60

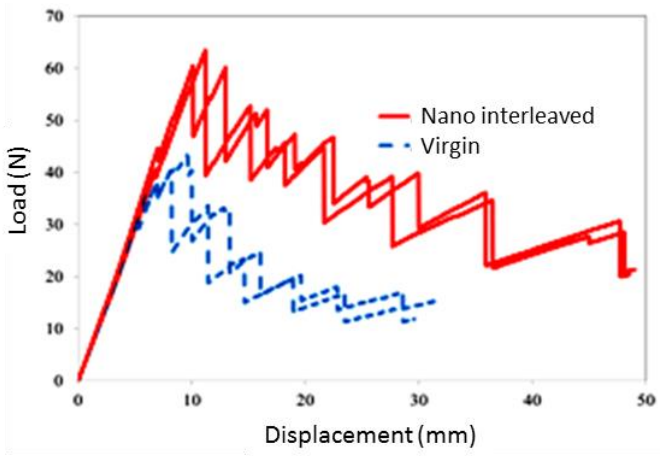

Figure 3. Load-displacement curves of the static tests.

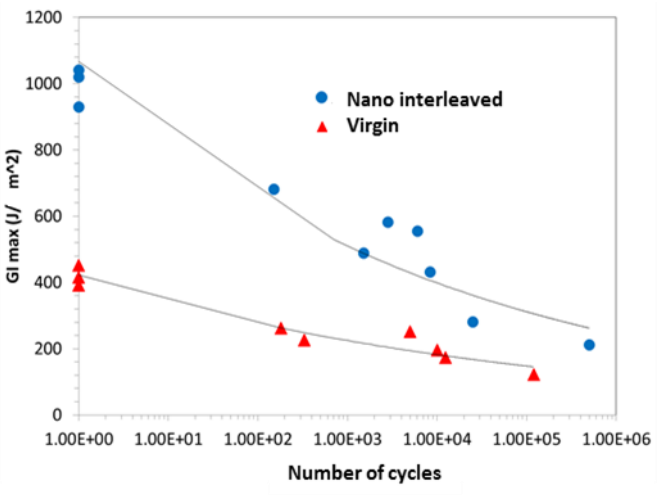

Figure 4. G_{Imax}-Na for the fatigue tests calculated based on ASTM D6115 [22]. G_{Imax} is the critical energy release rate that is required for the crack initiation under different number of cycles (Na).

3.2. AE results

Load-time and AE energy–time curves of a virgin sample is illustrated in Figure 5 as a representative of the investigated samples behavior. The load-time is presented instead of the load-displacement diagram to be able to present the mechanical and AE data in one graph. A similar trend was observed for the nano-interleaved samples, where two different stages are observable regarding the mechanical and AE behavior as illustrated in Figure 5.

1) Linear elastic region: this is before the initiation and propagation of delamination with no major damage in the specimens, therefore no change in mechanical data, such as stiffness, and no AE signals with high energy content.
2) Crack initiation and propagation: crack initiation is where the delamination initiates as the strain energy level reaches the critical strain energy in the laminates. Delamination onset is recognizable where the slope of the load curve versus time decreases (non-linearity point in ASTM5528 [21]) and the first significant AE signal is observable. In the propagation stage, the pre-crack is extended and considerable AE signals appeared from delamination extension and arrest, and therefore development of the failure mechanisms. Induced failure mechanisms generate different types of AE signals that can provide valuable information about the type of these failures. The crack arresting stage occurs when there is an increase in the load and therefore stored strain energy. When the strain energy attains the critical value, the crack propagates again and causes different types of damage modes such as fiber breakage, matrix cracking, etc.

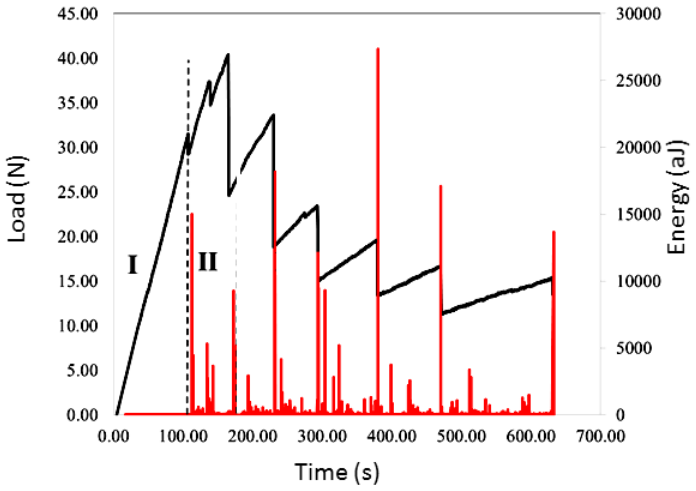

Figure 5. Load–time and AE energy time curves for the reference laminate.

This section analyzes the AE signals to recognize the failure modes. There is a wide literature about energy or amplitude based characterization of failure modes in composite laminates [27-33]. These studies represent various energy and amplitude domains for the damage modes. These studies reported that the high domains of energy, amplitude and frequency of AE signals are associated with fibre failure, while the middle and low domains are related to delamination/debonding and transverse/longitudinal crack of matrix, respectively. Therefore, three types of signals classification is presented in table 2 based on the recorded AE signals in this paper. This classification is according to previously published works in damage characterization of composite materials using AE [27-33].

Table 2. Classification of the AE signals based on their amplitude and energy content.

Signal type	Amplitude (dB)	Energy (aJ)
Matrix cracking	40–65	0–30
Debonding	60–85	30–800
Fibre failure	75–100	800–65,000

The received AE data are useful to realize the damage modes and help to understand the reason behind the improvement in the fracture toughness of the laminates. Figures 6 and 7 show the obtained AE signals classified based on the aforementioned criteria for the static and fatigue loadings, respectively. The AE events appeared in the virgin samples are higher than the nano interleaved samples (see Figure 6.b.). Matrix cracking related AE signals were less in the nano-interleaved samples compared with the virgin samples as well.

Comparing the damage mechanisms in the fatigue loading in Figure 7, the initial damage in the virgin sample is matrix cracking and debonding, whereas the damage in the nano-interleaved sample started with a higher amplitude that is associated with fibre breakage. It means that the toughness improvement in the modified samples is not due to the thicker resin area, and it is mainly due to the existence of tough Nylon 66 nanofibers.

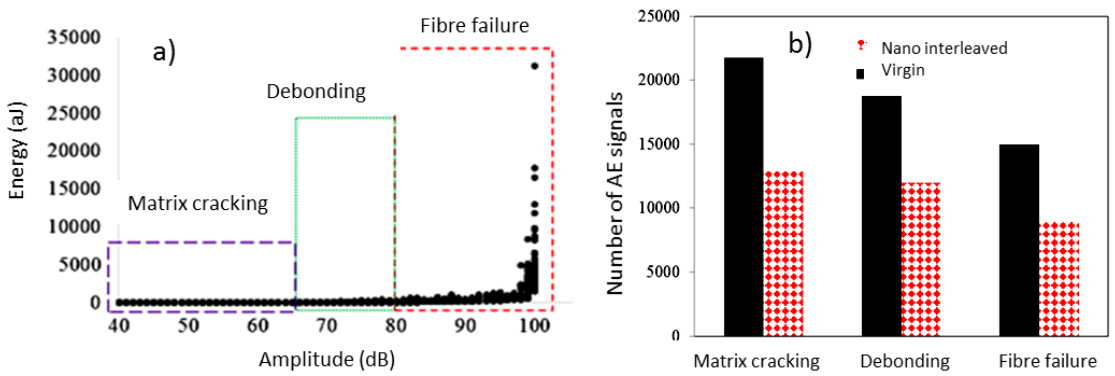

Figure 6: (a) Classification of the AE data by Energy and Amplitude levels, (b) Number of the AE signals associated with different damage modes for the static loading.

163

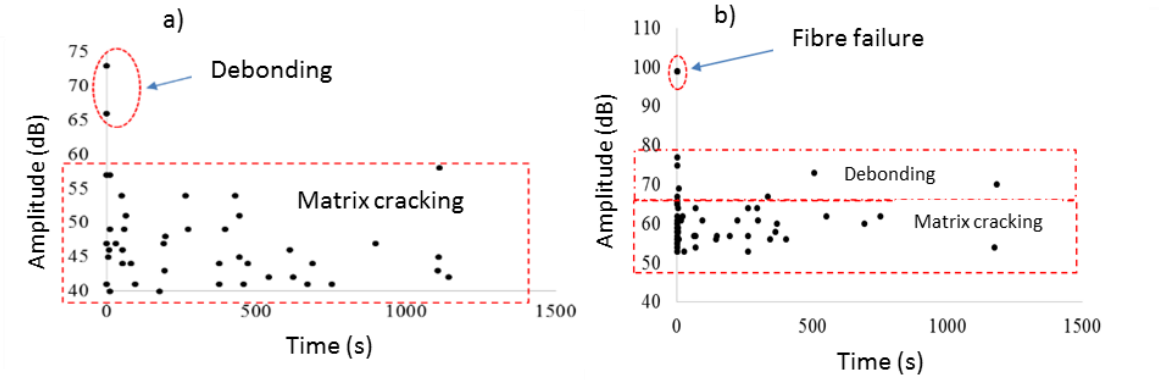

Figure 7. Amplitude versus time distribution of the AE signals for the fatigued samples (a) Virgin and (b) Nano-interleaved.

164

165 The morphology of the fractured surface for the virgin and nanomodified specimens is illustrated in
166 Figure 8. Fracture surface of the virgin specimen is mostly containing matrix cracking in the resin-
167 rich section near the fibers between two adjacent plies. On the other hand, fractured surface of the
168 nanomodified specimen is affected by the nanofiber interlayer, so a plastic zone occurred in front of
169 the crack tip during the crack growth.

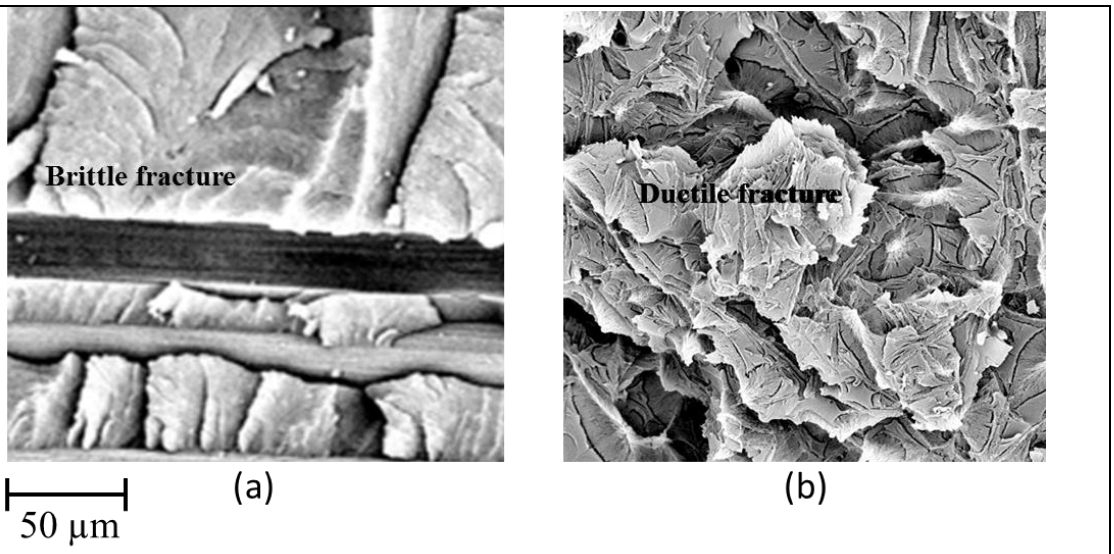

Figure 8. Morphology of the fractured surface for the a) virgin specimen and b) nano-modified samples under quasi-static loading.

5. Conclusions

This paper investigated the effect of Nylon 66 nanofibers reinforcement effect on interlaminar properties in mode I and resulted failure mechanisms of carbon/epoxy laminates under fatigue and static loadings. Static test (based on ASTM5528) and fatigue tests (based on ASTM D6115) were applied to the DCB specimens and the samples were monitored by the AE sensors during the tests. The mechanical results proved the effectiveness of the interleaved Nylon 66 nanofibre mate to improve fracture toughness in the delamination propagation and initiation stages for both of the static and fatigue loading conditions. The AE results showed that the number of interlaminar occurred failure modes reduced in the nano-interleaved samples. There were more matrix cracking associated AE signals in the virgin samples compared with the nano-interleaved samples. It means that the reason for the improved fracture toughness is due to the change in the appeared damage mechanisms that require higher energy level to initiate and propagate. Finally, it can be concluded that the nano-interleaved samples can improve the delamination resistance of laminated composites under static and fatigue loadings.

Conflicts of Interest: The author(s) declared no potential conflicts of interest with respect to the research, authorship, and/or publication of this article.

References

1. Tsai, G.C.; Chen, J.W. Effect of stitching on mode I strain energy release rate. *Compos Struct* **2005,**69,1–9.
2. Wong, D.W.Y.; Lin L.; McGrail, P.T.; et al. Improved fracture toughness of carbon Ebre/epoxy composite laminatesusing dissolvable thermoplastic Ebres. *Compos Part A Appl Sci Manuf* **2010**,41,759–767.
3. Wang, CH.; Sidhu, K.; Yang, T.; et al. Interlayer self-healing and toughening of carbon fiber/epoxy composites using copolymer films. *Compos Part A Appl Sci Manuf* **2012,** 43, 512–518.
4. Pavlovic, A.; Fragassa, C.; Disic, A. Comparative numerical and experimental study of projectile impact on reinforced concrete. *Compos Part B: Engineering* **2017**,108, 122–130.
5. Tang, G.; Yan. Y; Chen, X.; et al. Dynamic damage and fracture mechanism of three-dimensional braided carbon fiber/epoxy resin composites. *Mater Design*, **2001**,22,21–25.
6. Van, V.P.; Ballout, W.; Daoust, D.; et al. Influence of thermoplastic diffusion on morphology gradient and on delamination toughness of RTM-manufactured. *Compos Part A Appl Sci Manuf* **2015**,72,175–183.

7. Sohn, M.S.; Hu, X.Z.; Kim, J.K.; et al. Impact damage characterization of carbon fiber/epoxy composites with multi-layer reinforcement. *Compos Part B Eng* **2000**,31,681–691.
8. Wu X; Yarin AL. Recent progress in interfacial toughening and damage selfhealing of polymer composites based on electrospun and solution-blown nanofibers: an overview. J Appl Polym Sci **2013**,130(4).
9. Koissin V; Warnet LL; Akkerman R. Delamination in carbon-fibre composites improved with in situ grown nanofibres. Eng Fract Mech **2013**,101,140–148.
10. Daelemans L; van der Heijden S; De Baere I; Rahier H; Van Paepegem W; De Clerck K. Using aligned nanofibres for identifying the toughening micromechanisms in nanofibre interleaved laminates. Compos Sci Technol **2016**,124,17–26.
11. Yasaee, M.; Bond, I.P.; Trask, R.S.; et al. Mode I interfacial toughening through discontinuous interleaves for damage suppression and control. *Compos Part A Appl Sci Manuf* **2012,**43,198–207.
12. Saghafi, H.; Zucchelli, A.; Palazzetti, R.; Minak, G. The effect of interleaved composite nanofibrous mats on delamination behavior of polymeric composite materials. *Composite Structures* **2014**,109,41–47.
13. Brugo, T.M.; Minak, G.; Zucchelli, A.; Saghafi, H.; Fotouhi, M. An Investigation on the Fatigue based Delamination of Woven Carbon-epoxy Composite Laminates Reinforced with Polyamide Nanofibers. *Procedia Engineering* **2015**,109,65–72.
14. Fotouhi, M.; Saghafi, H.; Brugo, T.; Minak, G.; Fragassa, C.; Zucchelli, A.; et al. Effect of PVDF nanofibers on the fracture behavior of composite laminates for high-speed woodworking machines. *P I Mech Eng C-J Mec* **2017**,231,31-43.
15. Marec, A.; Thomas, J.H.; Guerjouma, E.R. Damage characterization of polymer-based composite materials: multivariable analysis and wavelet transform for clustering acoustic emission data. *Mech Sys Sig Proc* **2008**,22,1441–1464.
16. Uenoya, T. Acoustic emission analysis on interfacial fracture of laminated fabric polymer matrix composites. *J Acous Emiss* **1995**,13,95–102.
17. de Oliveira, R.; Marques, A.T.; Health monitoring of FRP using acoustic emission and artificial neural networks. *Comput Struct* **2008**,86,367–373.
18. Fotouhi, M.; Pashmforoush, F.; Ahmadi, M.; et al. Monitoring of initiation and growth of delaminationin composite materials using acoustic emission under quasi-static 3-point bending test. *J Reinf Plast Compos* **2011**,30,1481.
19. Pashmforoush, F.; Fotouhi, M.; Ahmadi, M. Acoustic emission-based damage classification of glass/polyester composites using harmony search k-means algorithm. *J Reinf Plast Compos* **2012,**31, 671–680.
20. Saeedifar, M.; Fotouhi, M.; Ahmadi, M.; et al. Prediction of delamination growth in laminated composites using acoustic emission and cohesive zone modeling techniques. *J Compos Struct* **2015,**124,120–127.
21. Fotouhi, M.; Ahmadi, M. Acoustic emission based study to characterize the initiation of mode I delamination in composite materials. *J Thermoplast Compos Mater* **2014,**519–537.
22. Bohse, J. Acoustic emission characteristics of micro-failure processes in polymer blends and composites *Compos Sci Technol* **2000,**60,1213-1226.
23. ASTM D5528. Standard test method for Mode I interlaminar fracture toughness of unidirectional fiber-reinforced polymer matrix composites. *Annual Book of ASTM Standards*, **2007**.
24. ASTM D6115. Standard Test Method for Mode I Fatigue Delamination Growth Onset of Unidirectional. *Annual Book of ASTM Standards*, **1997**.
25. Ishbir, C.; Banks-Sills, L.; Fourman, V.; Eliasi, R. Delamination propagation in a multidirectional woven composite DCB specimen subjected to fatigue loading. *Composites Part B: Engineering* **2014**,66,180–189.
26. Huang, M.; Jiang, L.; Liaw, P.K.; Brooks, Ch.R.; Seeley, R.; Klarstrom, D.L.; Using acoustic emission in fatigue and fracture materials research. *Nondestruct Eval Overview* **1998**,50,11.
27. Barré, S.; Benzeggagh, M.L. On the use of acoustic emission to investigate damage mechanisms in glass-fibre-reinforced poly-propylene. *Compos Sci Technol* **1994,**52,369-376.
28. Benmedakhene, S.; Kenane, M.; Benzeggagh, M.L. Initiation and growth of delamination in glass/epoxy composites subjected to static and dynamic loading by acoustic emission monitoring. *Compos Sci Technol* **1999**,59,201-208.
29. Guerjouma, R.E.; Baboux, J.C.; Ducret, D.; Godin, N.; Guy, P.; Huguet, S.; et al. Nondestructive evaluation of damage and failure of fiber reinforced polymer composites using ultrasonic waves and acoustic emission **Adv Eng Mater 2001**,3,601-608.
30. Woo, S.C.; Choi, N.S. Analysis of fracture process in single-edge-notched laminated composites based on the high amplitude acoustic emission events. *Compos Sci Technol* **2007** 67,1451-1458.

31. Palazzetti, R.; Zucchelli,A.; Gualandi, C.; Focarete, M.L.; Donati, L.; Minak, G. Influence of electrospun Nylon 6,6 nanofibrous mats on the interlaminar properties of Gr–epoxy composite laminates. *Compos Struct* **2012**,94,571-579.
32. Fotouhi ,M.; Ahmadi, M. Investigation of the mixed-mode delamination in polymer-matrix composites using acoustic emission technique. *J Reinf Plastic Comp* **2014**,33,1767-1782.
33. Fotouhi, M.; Suwarta, P.; Jalalvand, M.; Czel, G.; Wisnom, M.R. Detection of fibre fracture and ply fragmentation in thin-ply UD carbon/glass hybrid laminates using acoustic emission. *Compos A Appl Sci Manuf* **2016**, 10.1016/j.compositesa.2016.04.003.